Proceedings of Conference: ***Adapting to Change: New Thinking on Comfort*** Cumberland Lodge, Windsor, UK, 9-11 April 2010. London: Network for Comfort and Energy Use in Buildings, http://nceub.org.uk

Thermal comfort prediction under non-uniform heating conditions with physiological responses comfort model

Mengyin Wan[1], Tomonori Sakoi [3], Hideaki Nagano[1], Shinsuke Kato[2], Shengwei Zhu[4], Toshiaki Omori[5], and Akiko Okada[5], Ryozo Ooka[2]

[1] Graduate School of Engineering, The University of Tokyo, Tokyo, Japan
Corresponding email: wanmy@iis.u-tokyo.ac.jp
[2] Institute of Industrial Science, The University of Tokyo, Tokyo, Japan
[3] Shinshu University, Nagano, Japan
[4] Harvard University, Boston, USA
[5] Tokyo Gas Co., Ltd. Tokyo, Japan

Abstract

This research aims to use a highly accurate thermal comfort prediction method that links non-uniform environments to the body's thermal sensation by numerical simulation. In order to predict the thermal sensation of an occupant in non-uniform environments with floor heating and air conditioning, we performed local and whole body thermal comfort evaluations through coupled simulation of a thermal comfort model considering body segmental characteristics of physiological responses.

With the coupled simulation, the skin temperature distribution and sensible heat loss of simulation results were used to calculate the Ratio of whole-body thermal Comfort Sensation, (*RCS*) (T Sakoi et al. 2005b), which was taken as the evaluation criteria for whole body thermal comfort. It indicated that the temperature distribution of human body regions was more uniform with floor heating than air conditioning. In addition, the *RCS* of the floor heating system was 4% higher than that of the air conditioning system.

Keywords

non-uniform environment, thermal comfort, thermal physiological model, thermal sensation

1. INTRODUCTION

Taking advantage of non-uniform radiant environments, such as cooling/heating

panels, floor heating has been widely used in recent years. One of the most important targets is to improve thermal comfort. Besides the experimental method using an experimental manikin or human subjects, coupled simulation of computational fluid dynamics (CFD), radiation, moisture transport, and heat transfer inside the human body has been accepted as a more economical and effective tool for examinations of thermal sensation.

The human thermal physiological models in the studies of Fanger (1973) and Gagge et al. (1971) dealt with whole-body heat balance rather than local balance. Because thermal sensation is highly dependent on local heat transfer characteristics, the multi-element human thermal physiological model developed by Smith (1991), which has a three-dimensional (3D) shape and can produce 3D temperature distributions, was adopted. Additionally, in order to generate arteriovenous anastomose (AVA) blood flow at the limbs, a new human thermal physiological model, Sakoi's model (T Sakoi et al. 2005a, 2006a), was developed. The blood circulatory system is remodeled as in Stolwijk's (1971) model, with the blood perfusion rate for skin tissue changed numerically under a fixed volume of vessels.

In this paper, Sakoi's model is adopted in the coupled simulation to express the thermal condition in a sitting posture in non-uniform thermal environments of air conditioning and floor heating. An evaluation method for whole-body thermal comfort based on the relationships between thermal comfort, local thermal state, and local heat loss was used to predict thermal comfort in different kinds of environments.

2. EVALUATION METHOD

The validity of thermal indices expressed in local environmental temperature, which signifies the influences of multiple local thermal factors, such as partial operative temperature and local equivalent temperature, etc., was investigated in order to evaluate the non-uniform thermal environment. It was ascertained that due to a variety of heat transfer rates at skin surfaces, these indices can express local thermal states only under limited conditions.

In order to evaluate the overall thermal comfort under non-uniform environments, according to Sakoi et al. 2005, the *RCS* can be calculated by Eq. (1). We assume that for the narrow range of thermally comfortable conditions, ‘‘Comfortable’’ and “Uncomfortable” are located symmetrically either side of “Neither comfortable nor uncomfortable.” It can be supposed that the higher the *RCS*, the higher the thermal comfort level of the environment is. From the equation, the maximum and minimum *RCS*es are 1.0 and 0.0.

RCS = + 1.0 × percentage “Comfortable”

+ 0.5 × percentage “Neither comfortable nor uncomfortable”

+ 0.0 × percentage “Uncomfortable” (1)

The empirical formula of *RCS* was given based on human subject experiments under various kinds of non-uniform environments. First, the thermal conditions of human body parts are considered to be a function of the skin temperature and sensible heat loss of the parts respectively. Here the minimum division of seven parts was used. Since Sakoi’s model divided the human body into 32 parts, the correspondence relationship is listed in Table 1.

$$F_{\mathrm{i}} = \frac{T_{sk\mathrm{i}} - B}{\Delta + Q_{sk\mathrm{i}}} \tag{2}$$

F_{i} : indicator of local thermal sensation [N.D.];

$T_{sk\mathrm{i}}$: local skin temperature [°C];

$Q_{sk\mathrm{i}}$: local sensible heat loss [W/m^2];

B is a constant in °C, Δ is a constant in W/m^2, and subscript *i* corresponds to local segment *i*.

The mean value of the function F_{i} for the whole body F_{T}' can be calculated by Eq. (3).

$$F_{\mathrm{T}} = \sum_{\mathrm{i}} F_{\mathrm{i}}^{'} \cdot W_{\mathrm{i}} \tag{3}$$

F_{T} : mean value of the function F_{i} for the whole body [N.D.];

W_i : weighted coefficient of skin area of human body parts i [N.D.];

The ratio of whole-body thermal comfort RCS is expressed using the term β and χ in Eq. (4). The term β reflects thermal discomfort effect brought by sensation of heat and sensation of cold for the whole body. The term χ reflects thermal discomfort effect brought by a distribution of local thermal sensation different from a distribution leading to the maximum thermal comfort.

$$RCS = \beta(F_T) \cdot \chi\left(\frac{F_1}{F_T}, \frac{F_2}{F_T}, \frac{F_3}{F_T}, \cdots \frac{F_p}{F_T}\right) \tag{4}$$

The term β can be expressed in Eq. (5). It depends only on F_{T}, and takes its maximum value α_β at $F_{\mathrm{T}} = \delta/2$, and becomes less as the absolute value of $|F_{\mathrm{T}} - \delta/2|$ becomes larger.

$$\beta = \alpha\beta \frac{F_T^{nT} \left(\delta - F_T\right)^{nT}}{\left(\delta/2\right)^{2nT}} \tag{5}$$

where α_β, δ and nT are constants in N.D.

The term χ is expressed as shown in Eq. (6). It takes its maximum value at a fixed distribution of $W_i \cdot F_i$ ($W_1 \cdot F_1$: $W_2 \cdot F_2$: ⋯: $W_p \cdot F_p$=m_1: m_2: ⋯: m_p).

$$\chi = \alpha\chi \cdot \left(\frac{W1 \cdot F1}{FT}\right)^{m1} \cdot \left(\frac{W2 \cdot F2}{FT}\right)^{m1} \cdot \left(\frac{W2 \cdot F2}{FT}\right)^{m1} \cdots \left(\frac{Wp \cdot Fp}{FT}\right)^{mp} \quad (6)$$

where $\alpha\chi$ and m_i are constants in N.D. (furthermore, mi >0).

Thus, taking into account the discomfort caused by the non-uniform compared to uniform distribution of the human body thermal condition, *RCS* is expressed by Eq. (7).

$$RCS = \alpha_\beta \cdot \frac{F_T{}^{nT} \cdot (\delta - F_T)^{nT}}{(\delta/2)^{2nT}} \cdot \alpha_\chi \cdot \left(\frac{F_1}{F_T}\right)^{m1} \cdot \left(\frac{F_2}{F_T}\right)^{m2} \cdot \left(\frac{F_3}{F_T}\right)^{m3} \cdots \left(\frac{F_p}{F_T}\right)^{mp} \quad (7)$$

All of the constants were set based on experiments (Tomonori Sakoi et al. 2007) and are listed in Tables 1 and 2.

Table 1 Division of Human Body Model in RCS calculation and CFD Simulation Constants of W_i , m_i

7 Body parts of RCS	32 Body parts of Sakoi Model	W_i	m_i
Head	face head neck-front neck-back	0.110	4.95
front trunk	chest-right chest-left waist-right-front waist-left-front	0.134	4.67
back trunk	back-right back-left waist-right-back waist-left-back	0.168	6.37
Right arm	upper arm-right-front upper arm-right-back forearm-right-front forearm-right-back right hand	0.104	2.78
Left arm	upper arm-left-front upper arm-left-back forearm-left-front forearm-left-back left-hand	0.104	2.95
Right leg	thigh-right-front thigh-right-back leg-right-front leg-right-back foot-right	0.190	5.81
Left leg	thigh-left-front thigh-left-back leg-left-front leg-left-back foot-left	0.190	5.58

Table 2 constants in Equation (2) to (6)

B	Δ	α_β	$\alpha\chi$	δ	n_T
25.0	246.6	0.757	0.814	0.0591	12.77

3. OUTLINE OF SIMULATION

Introduction of Sakoi Model

As shown in Figure 1(a), in Sakoi's model, the 3D shape of Smith's model is adopted and the whole body is also approximated geometrically by 15 cylindrical body parts (head, neck, torso, upper arms, thighs, forearms, calves, hands, and feet). However, in Sakoi's model each body part is divided into more detail to obtain a more accurate 3D temperature distribution, and the whole body is made up of 2,744 3D (triangular or rectangular) tissue elements. Each tissue element is designated as a specific type, such as brain, bone, lung, viscera, muscle, fat or skin, with a corresponding physical property following that proposed by Smith.

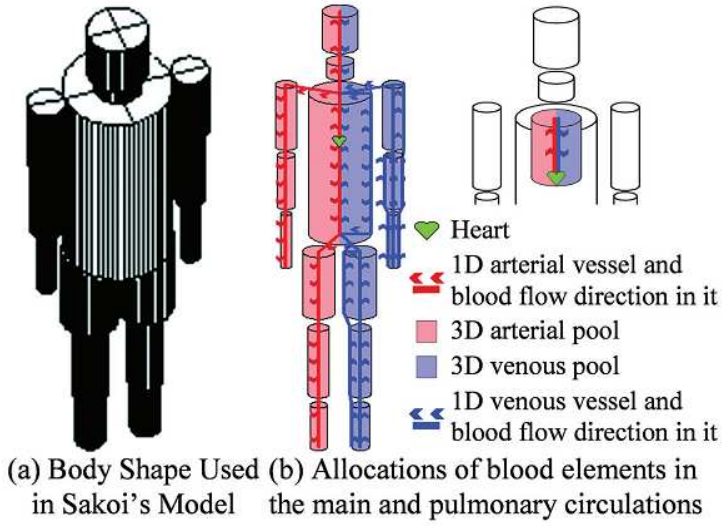

Fig. 1 Image of Sakoi's model

Figure 1(b) illustrates the vascular networks. The blood flow is not controlled by the dilation and constriction of vessels in the model; rather, its perfusion rate for skin tissue changes numerically under the fixed volume of the vessel.

In conclusion, Sakoi's model (Sakoi et al. 2005a, 2006a) is the only human thermal physiological model that can accomplish the following four points simultaneously: 1) blood mass is conserved despite vasoconstriction and vasodilation, 2) 3D temperature distribution is produced in the human body, 3) hot conditions provoke an increase in

the blood flow rate through the superficial veins, and 4) thermal conduction in the subcutaneous fat layer is calculated directly using temperature difference in this layer and the thickness and thermal properties.

Coupled Simulation Method

Figure 2 illustrates an overview of the coupled simulation method. Here, Sakoi's model accounts for the simulation of internal heat transfer of the human body. The skin temperature is obtained for each external element by calculation of the inner heat conduction, which uses sensible (convective and radiant) heat transfer rates determined by means of a coupled simulation of the flow field, radiation, and moisture transport as boundary conditions, as does the sweat rate generated from the skin. However, the sweat rate is calculated using the method from Smith's (1991) model in this study, because it is impossible to directly get the convective heat transfer coefficient during the simulation, which is used to calculate the saturation steam pressure on the skin surface to evaluate the influence of the airflow around the human body in Sakoi's original model. It should be noted that Smith's model calculates the sweat rate based on Fanger's (1973) model. The latent heat transfer over the human body is calculated based on the sweat rate distribution.

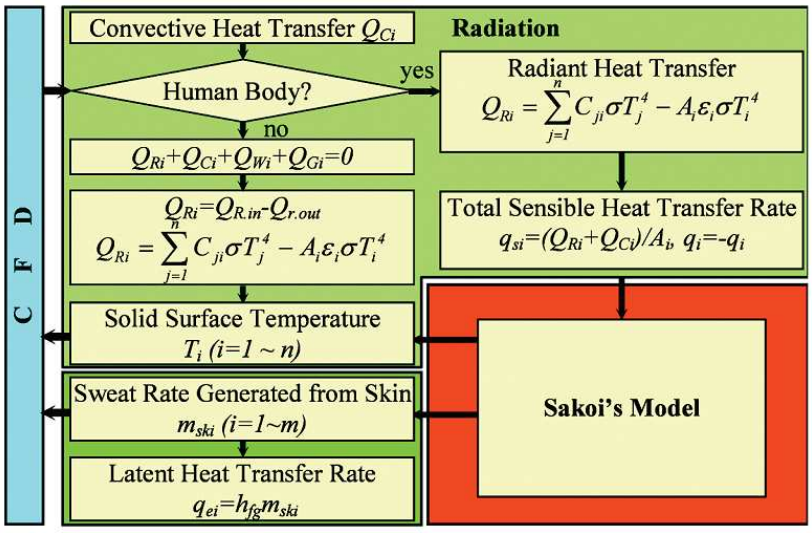

Fig. 2 Overview of coupled simulation method.

Geometry of Simulation Model Analyzed

As shown in Figure 3, the field analyzed is a model of an experiment chamber in the Institute of Industrial Science at the University of Tokyo. A person in short was assumed to be sitting at the center of the room (1,800 mm × 1,800 mm × 2,550 mm) with radiant panels set to her front. The cooling panel simulated a cool window in

winter. There is an inlet on her right hand side, at the bottom of the room while the outlet is at the top of the room. All the enclosure structures are well insulated. A floor heating system is set to control the temperature of the floor.

Cases Analyzed

As shown in Table 3, three cases were simulated. In Case 1, a uniform radiant condition was selected by setting the radiant panel to the same temperature as the room air. In Case 2, the air conditioning (heating) environment was examined, as inlet airflow was set at 33°C, and the radiant panel (simulating a cool window) was set at 10°C. In Case 3, the floor heating environment was examined, with the floor temperature set at 28°C, inlet flow at 16°C with an air exchange rate of 1.0/h for ventilation.

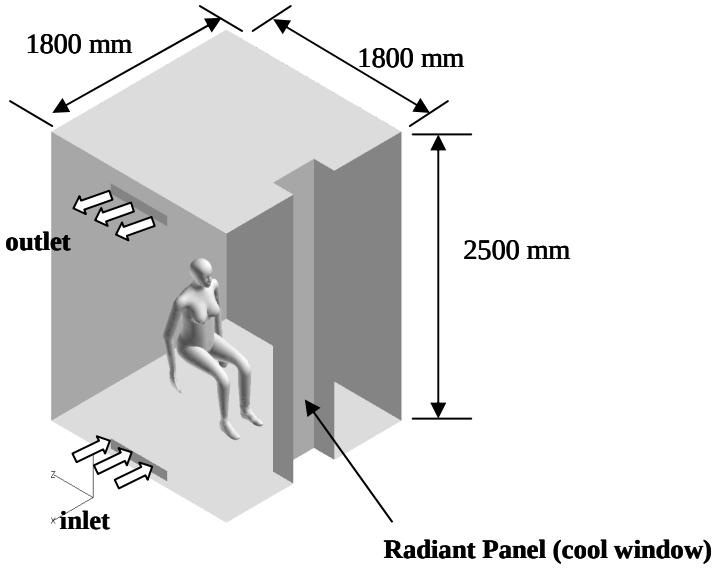

Fig. 3 Analysis flow field

Table 3. Cases Analyzed

Case No.	Condition	Temperature of Airflow	Temperature of Panel	Temperature of Floor	Temperature of Other Walls
1	Uniform radiant condition With Air Conditioning	28°C	adiabatic	adiabatic	adiabatic
2	Cooling Panel With Air Conditioning (heating)	33°C	10°C	adiabatic	adiabatic
3	Cooling Panel With Floor Heating and Ventilation	16°C	10°C	28°C	adiabatic

Grid System

There were 17498 triangular surface meshes and 220,935 spatial cells used. As shown in Figure 4, prism-shaped fluid cells were used for the first, second, and third cell layers placed over the whole surfaces, while the rest of the flow field was filled with tetrahedral meshes.

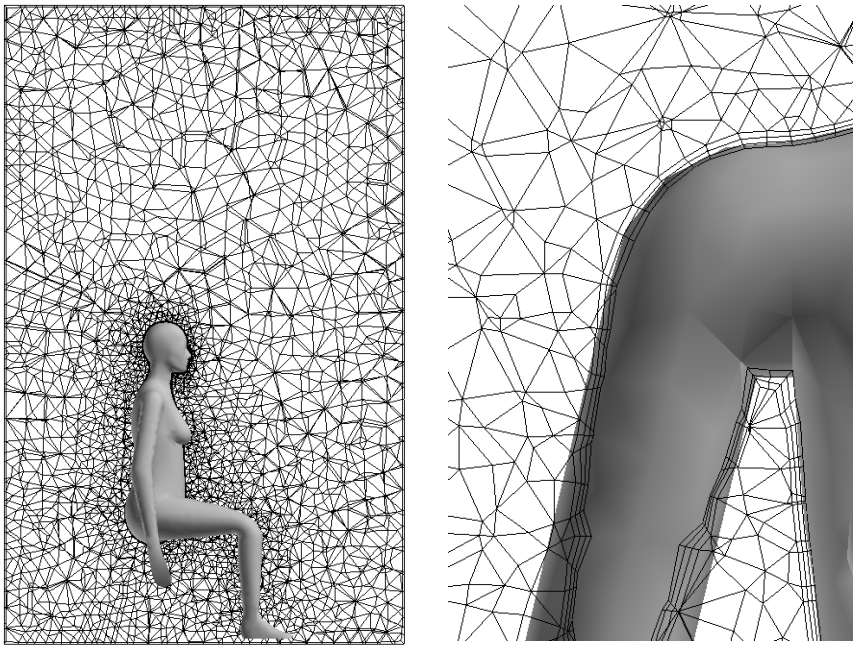

Fig.4 Cells around human body model.

Simulation Conditions

The CFD boundary conditions are shown in Table 4. Except for the skin surfaces, other wall surfaces were defined as completely insulated in terms of humidity. In the radiant calculation, emissivity was set uniformly at 0.95 for all boundary surfaces. During coupled Simulation using Sakoi's model, the metabolic heat production was set as 59.1 W/m^2.

The skin temperatures based on Sakoi's model are used as the boundary conditions for the surface meshes of the human body model in the CFD method, where a low-Reynolds-number type k-ε turbulence model (Lien, F.S. et al. 1996) is adopted together with the SIMPLE algorithm and the monotone advection and reconstruction scheme (MARS, a second-order scheme, van Leer et al. 1979) for convection terms. Thermal radiation is calculated using Gebhart's absorption factor method, and the configuration factors over the complex geometry are accurately calculated using the Monte-Carlo method (Howell, J.R. et al 1964), incorporating symmetrization procedures (Omori, T. et al. 1998, 2004).

4. SIMULATION RESULTS

Velocity Distribution

Figure 5 shows the velocity distribution in each case. In Case 1, air was heated by the warm body so that it accelerated upwards and reached a maximum velocity of about 0.2 m/s above the head. The flow in the room above the human body is almost stagnant with an ascending airflow of 0.05 m/s. In Cases 2 and 3, inflow air rose due to buoyancy upon mixing with the room air. Meanwhile, a descending flow was found near the cooling panel. Thus the airflow around the human body was not as stable as in Case 1. Compared to Case 2, the air velocity above the head and under the thighs was higher in Case 3.

Table 4.Boundary Conditions and Method of CFD

Inlet		Size: 0.605m×0.121m;
	Case 2	Velocity: 0.2m/s; Temperature: 33°C
	Case 3	Velocity: 0.03m/s; Temperature: 16°C
Outlet		Size: 0.605m×0.121m; Velocity and temperature: free-slip
Radiant Panel		Velocity: no-slip; Temperature: fixed values as shown in Table 3; humidity insulation
Skin Surfaces		Velocity: no-slip; Temperature and sweat rate: calculation results from Sakoi's model
Other Wall Surfaces		Velocity: no-slip; Temperature: results from radiant calculation, humidity insulation

Turbulence Model	Low-Reynolds-number type k-ε turbulence model
Algorithm	SIMPLE
Space Scheme	Velocity terms: MARS; scalar terms: first-order upwind

Air Temperature Distribution

Figure 6 illustrates the air temperature distribution in each case. In Case 1, the air temperature was almost uniform at 26°C across the whole room, except for the region closest to the human body, where air was heated by body warmth. In Case 2, the air temperature close to the feet was around 23°C. Above the human body, warm inflow

mixed with the cold air so that the air temperature rose to 27°C. In Case 3, the temperature gradient close to the radiant panel was almost the same as Case 2. However, the region where the air temperature was under 23°C near the feet in Case 3 was smaller than that in Case 2. The reason was likely to be the effect of the floor heating that warmed the descending air in front of the radiant panel, while in Case 2 although the warm air inflow was close to the floor, it ascended immediately without mixing well with the cold air around it. However, the air temperature under the thighs in Case 3 was lower than that in Case 2.

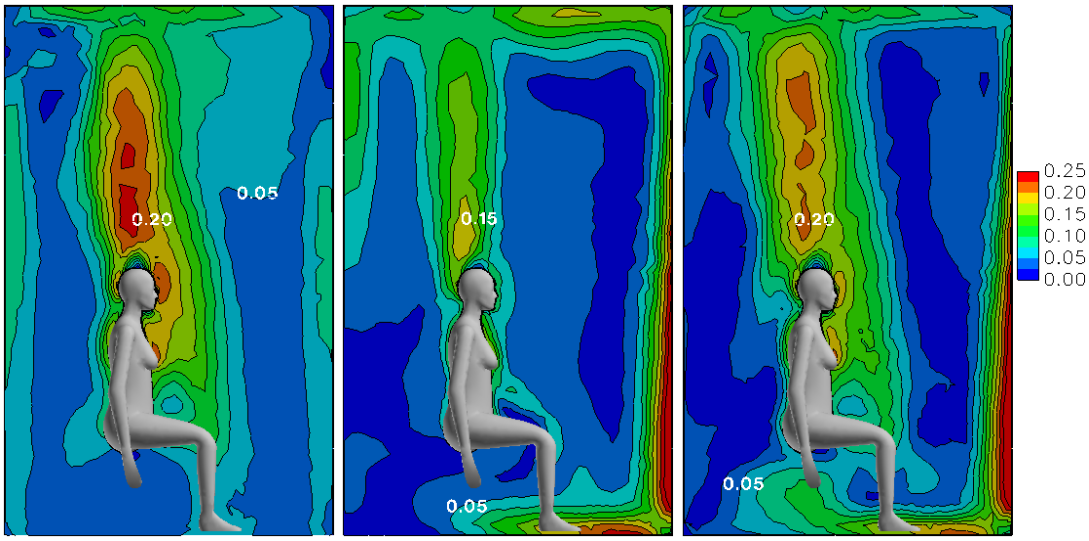

(a) Case 1 (b) Case 2 (c) Case 3

Fig. 5 Distribution of scalar velocity (m/s)

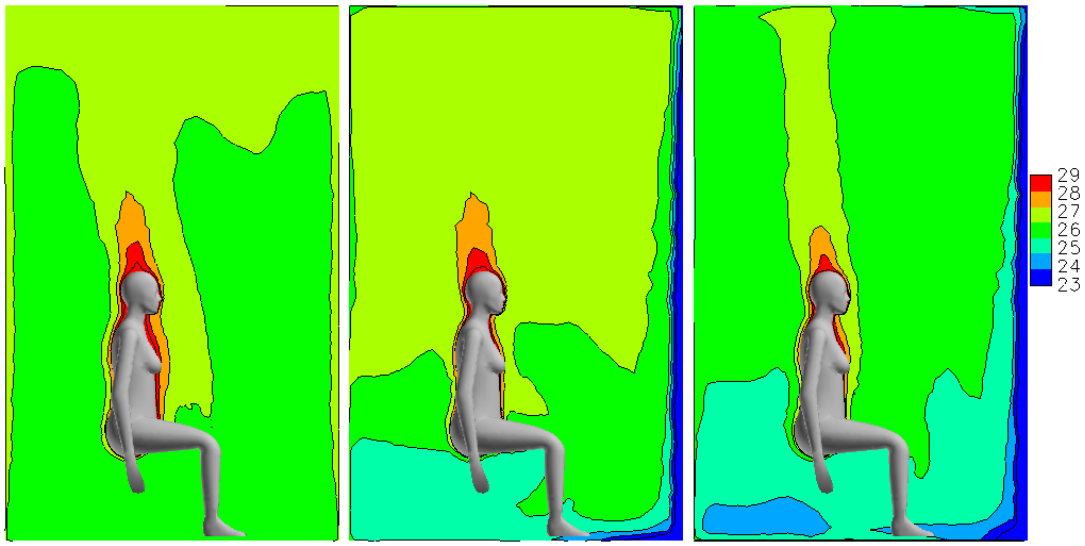

(a) Case 1 (b) Case 2 (c) Case 3

Fig. 6 Distribution of air temperature (°C)

Skin Temperature Distribution

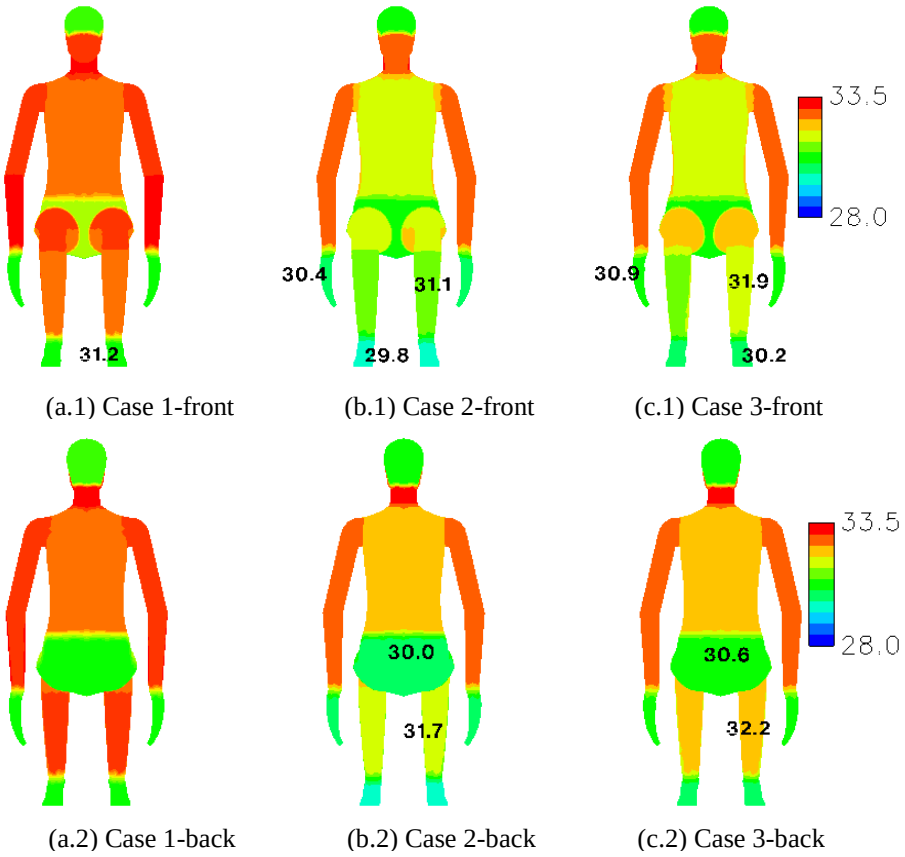

(a.1) Case 1-front (b.1) Case 2-front (c.1) Case 3-front

(a.2) Case 1-back (b.2) Case 2-back (c.2) Case 3-back

Fig. 7 Distribution of skin temperature (°C)

Figure 7 shows the skin temperature distribution over the human body. The average skin temperature of each part of the body was posted instead of every skin surface grid temperature. It can be clearly seen that the distribution in Case 1 was more uniform than that in other cases, distributed around 33°C. In Case 2, as shown in Figure 7-(b), the skin temperatures of hands and feet were appeared to be quite lower than other parts, which was 30.4°C and 29.8°C. Although skin temperature distribution in Case 2 was similar to Case 3, the skin temperatures of hands and feet were 0.5°C higher than those in Case 2 for the same parts. Comparing the front and back sides in each case, when the human body faced the cold panel, skin temperatures on the side near the cold panel tended to be lower than on the other side. For example, in Cases 2 and 3, the back of the legs was about 0.5°C higher than the front.

Total Sensible Heat Transfer Rate Distribution

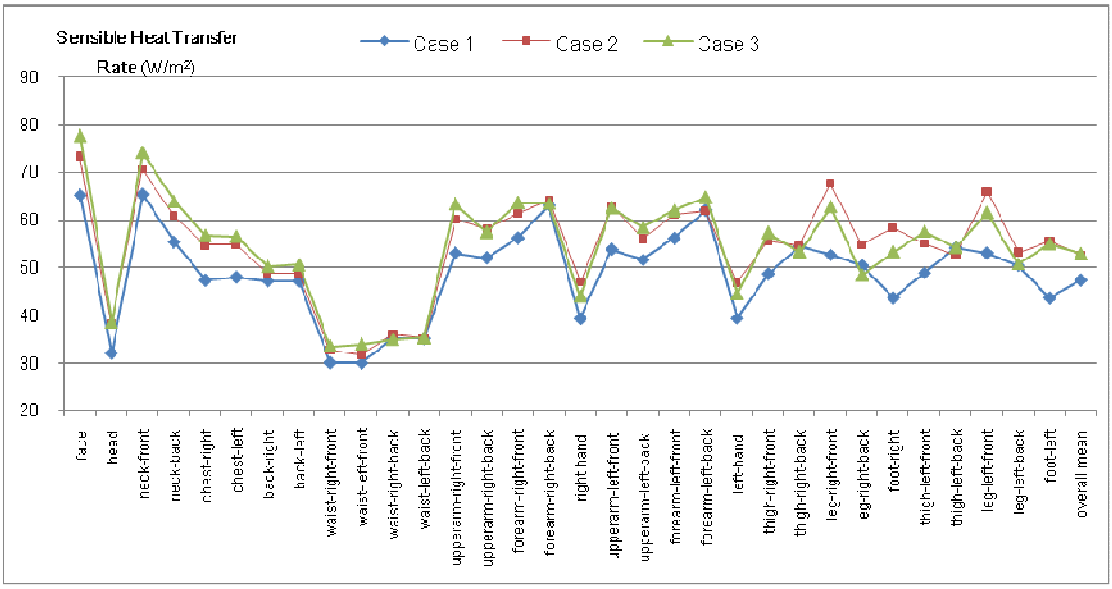

Fig. 8 Total Sensible Heat Transfer Rate Distribution (°C)

Figure 8 shows the distribution of the total sensible heat transfer rate both locally and for the overall human body in each case. In Case 1, the total heat transfer rate was maximized at the nose tip with a value of 65.4 W/m^2 and minimized around the crotch with a value of 29.9 W/m^2, and the overall mean value was 47.4 W/m^2. In Cases 2 and 3, compared to Case 1, total sensible heat transfer rates increased at the body surface facing the cold panels and decreased at the body surface closer to the supplied warm air or heated floor. Moreover, in Cases 2 and 3, total sensible heat transfer rates of the whole body were the same at 52.7 W/m^2. This demonstrates that the same sensible heat was released from the human body in Case 1 and Case 2.

5. PREDICTION OF OVERALL COMFORT SENSATION

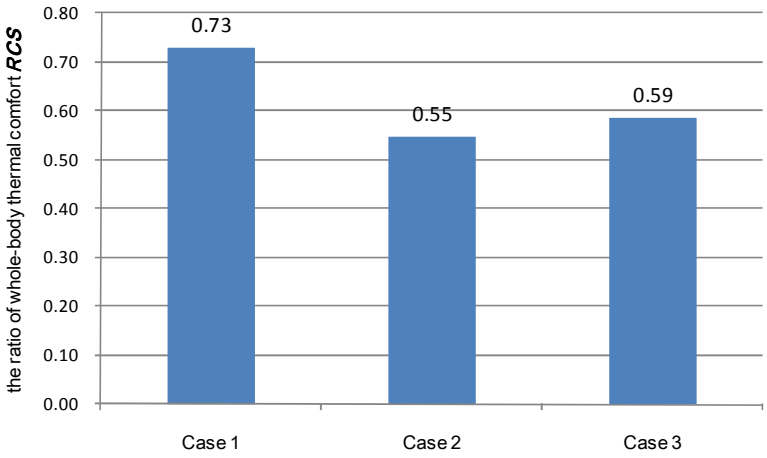

Fig. 9 Ratio of whole-body thermal Comfort Sensation *RCS* [N.D.]

The ratios of whole-body thermal comfort *RCS* in each case were calculated by Eq. (2), (3), (4) and shown in Figure 9. The *RCS* for Case 1 turned out to be the highest, with a value of 0.73, indicating 73% of people would likely feel comfortable under a uniform environment. In Cases 2 and 3, the *RCS* values were quite a bit lower than in Case 1, which was supposed to be affected by non-uniform environments. Compared to Case 2, the *RCS* of Case 3 was 4% higher, which indicated that the floor-heating environment was more comfortable.

6. CONCLUSIONS

1. This study proposed a method of predicting thermal sensation when a human body is subjected to different non-uniform heating conditions. Adopting Sakoi's model, incorporated in a coupled simulation of CFD, the skin temperature and sensible heat transfer rate from a human body, as well as overall comfort sensation, were calculated and compared between each case.

2. The results indicate that under different non-uniform environments, the distribution of air velocity and temperature in the room affected the human body thermal state greatly. When the human body faced the cold panel, skin temperatures on the side near the cold panel became lower than on the other side. Additionally, when the floor was heated, the foot and leg skin temperatures became higher than when the air conditioning system was used.

3. In terms of the human body thermal state, we calculated the overall comfort sensation, which is a function of skin temperature and sensible heat loss, for each part respectively. The result indicated that under the same overall mean sensible heat transfer rate, the ratio of overall thermal comfort using floor heating was about 4% higher than with air conditioning. Beside measurements and human subject experiments, it can be accepted that with coupled simulation of CFD and human thermal physiological models, we can predict the human body thermal state and then evaluate the thermal comfort level for a given environment.

4. In future studies, the factors below should be considered to develop the coupled simulation method into a more sufficient and useful tool to evaluate thermal sensation: 1) development of a clothing model accounting for convection and moisture transport with clothes on and evaluation of the influence of clothing asymmetry; 2) improvement in the prediction of overall thermal sensation considering different local thermal sensitivities; and 3) thermal comfort evaluation of different heating systems in an actual residential house.

ACKNOWLEDGEMENTS

The authors would like to express their gratitude to Dr. Kazuyo Tsuzuki of National Institute of Advanced Industrial Science and Technology, Japan, for her generous support and meaningful suggestions for this study.

REFERENCES

Fanger, P.O. 1973. Thermal sensation–Analysis and applications in environmental engineering. New York: McGraw-Hill.

Gagge, A.P., J.A.J. Stolwjik, and Y. Nishi. 1971. An effective temperature scale based on a simple model of human physiological regulatory response. ASHRAE Transactions 77(1):247–62.

Howell, J.R., and M. Perlmutter. 1964. Monte Carlo solution of thermal transfer through radiation media between gray walls. Transactions of ASME 86:116–22

Lien, F.S., W.L. Chen, and M.A. Leschziner. 1996. Low-Reynolds-number eddy-viscosity modeling based on non-linear stress-strain/vorticity relations. Proceedings of 3rd Symposium on Engineering Turbulence Modeling and Measurement, pp.1–10.

Omori, T., S. Yamaguchi, and H. Taniguchi. 1998. Accurate Monte Carlo simulation of radiative heat transfer with unstructured grid systems. Proceedings of the 11th International Symposium on Transport Phenomena, pp.567–73.

Omori, T., J.H. Yang, S. Kato, and S. Murakami. 2004. Coupled simulation of convection and radiation on thermal environment around an accurately shaped human body. Proceedings of the 9th International Conference on Air Distribution in Rooms.

Sakoi, T., K. Tsuzuki, S. Kato, R. Ooka, D. Song, and S.W. Zhu. 2005a. Development of a three-dimensional human thermal model accounting for direction of blood flow. Proceedings of the 3rd International Conference on Human-Environment System, paper number P-005, pp. 337–42.

Sakoi, T., K. Tsuzuki, S. Kato, R. Ooka, D. Song, and S.W. Zhu. 2005b. Proposal of expression of whole-body thermal sensation in non-uniform thermal environment. Proceedings of the 10th International Conference on Indoor Air Quality and Climate, pp.193–98.

Sakoi, T., K. Tsuzuki, S. Kato, R. Ooka, D. Song, and S.W. Zhu. 2006a. A three-dimensional human thermal model for non-uniform thermal environment. Proceedings of the 6th International Thermal Manikin and Modeling Meeting, pp. 77–88.

Sakoi, T., K. Tsuzuki, S. Kato, R. Ooka, D. Song, and S.W. Zhu. 2006b. Expression of thermal comfort in non-uniform thermal environments in terms of local skin

temperature and local dry heat loss. Proceedings of Healthy Building 2006, paper number P.412.

Smith, C.E. 1991. A transient three-dimensional model of the human thermal system. PhD dissertation, Kansas State University, Manhattan, KS.

Stolwijk, J.A.J. 1971. A mathematical model of physiological temperature regulation in man. NASA Contractor Report 1855, National Aeronautics and Space Administration, Washington, DC.

Tomonori Sakoi, Kazuyo Tsuzuki, Shinsuke Kato, Ryozo Ooka, Doosam Song, Shengwei Zhu. 2007. Thermal comfort, skin temperature distribution, and sensible heat loss distribution in the sitting posture in various asymmetric radiant fields. Building and Environment 42(2007): 3984–3999.

van Leer, B. 1979. Toward the ultimate conservation difference scheme II: Monotonicity and conservation combined in a second order scheme. Journal of Computational Physics 32:101–36.